Journal of Alloys and Compounds 806 (2019) 327–334

Contents lists available at ScienceDirect

Journal of Alloys and Compounds

journal homepage: http://www.elsevier.com/locate/jalcom

The role of DUV laser irradiation in the optical and electrical properties of indium zinc oxide films synthesized by self-combustion

Peng Li [a], Jun Duan [a], Jiangang Ma [a, *], Tingfeng Wang [b, c], Haiyang Xu [a], Yichun Liu [a]

[a] Key Laboratory for UV-Emitting Materials and Technology of Ministry of Education, Northeast Normal University, 5268 Renmin Street, Changchun, 130024, PR China
[b] State Key Laboratory of Laser Interaction with Matter, Changchun Institute of Optics, Fine Mechanics and Physics, Chinese Academy of Sciences, Changchun, 130024, PR China
[c] University of Chinese Academy of Sciences, Beijing, 100049, PR China

ARTICLE INFO

Article history:
Received 20 November 2018
Received in revised form
10 June 2019
Accepted 15 July 2019
Available online 16 July 2019

Keywords:
Transparent conducting film
Indium zinc oxide
Low temperature
Laser irradiation
Solution combustion

ABSTRACT

Highly conductive and transparent amorphous IZO films were fabricated by combining deep ultraviolet (DUV) excimer laser irradiation with solution combustion synthesis at low temperature. The influence of laser energy densities on the crystallinities, surface morphologies, and optical and electrical properties of the IZO films was investigated by using X-ray diffraction, scanning electron microscope, atomic force microscope, UV–vis spectroscopy, and Hall test. Additionally, Fourier-transform infrared spectroscopy showed that DUV laser irradiation led to the removal of organic residuals and hydroxyl groups. X-ray photoelectron spectroscopy showed that the percentage of metal–oxide–metal bonds in the IZO films increased significantly after the laser irradiation, which was beneficial for the electron transportation. As a result, the IZO films exhibited resistivity as low as $4.2 \times 10^{-3}\,\Omega\,cm$ with average visible transmittance as high as 91%, which yielded the highest Figure of Merit among the solution-processed transparent conducting films prepared at a temperature as low as 200 °C.

1. Introduction

Oxide materials are becoming increasingly important in a wide range of applications including transparent electronics and optoelectronics [1]. Among them, transparent conductive metal oxides are necessary component in optoelectronic devices such as liquid crystal displays, organic light emitting diodes, solar cells, optical sensors etc. [2,3]. Particularly, amorphous ternary metal oxide semiconductors (MOSs) possess spherically symmetric heavy-metal cation ns orbitals with $(n–1)d^{10}ns^0$ $(n \geq 4)$ electronic configurations. The adjacent spherically orbitals may overlap and form well-defined conduction paths [4]. In addition, amorphous MOSs fabricated at low-temperature have ultra-smooth surfaces and are devoid of grain boundaries. Those features can suppress interface trap centers and obviate the primary limitation of mobility in polycrystalline semiconductors. Thus, amorphous MOSs exhibit a stimulating combination of high optical transparency, high electron mobility, and ease of process integration [5].

Amorphous MOSs can be prepared by vacuum deposition methods such as magnetron sputtering and pulse laser deposition, as well as by chemical synthesis such as sol-gel [6–12]. A pioneering work reported by Raniero et al. demonstrated that magneton supporting can be used to prepare high-performance transparent conductive oxide at room temperature [8]. Gonçalves and co-workers investigated the electrical, structural, morphological, and optical properties of transparent conductive oxide films as a function of annealing temperature [9]. Fortunato et al. reported that indium zinc oxide (IZO) film deposited at room temperature exhibited an electron mobility as high as $60\,cm^2/V$ [10]. Lyubchyk and colleagues have fabricated aluminum zinc oxide (AZO) films with a high average visible optical transmittance around 88%, and a low resistivity of $3 \times 10^{-4}\,\Omega\,cm$ [11]. Compared with vacuum deposition, sol-gel method possesses advantages of simple equipment, easy composition adjustment, and low-cost manufacturing. Additionally, sol-gel method provides the possibility of directly patterning MOS films and avoiding complicated photolithography process. However, a high annealing temperature (usually ≥400 °C) is required to obtain transparent conducting films with low electrical resistivity ($<10^{-3}\,\Omega\,cm$) in the conventional sol-gel methods [12]. High annealing temperature is incompatible with

* Corresponding author.
E-mail address: majg@nenu.edu.cn (J. Ma).

https://doi.org/10.1016/j.jallcom.2019.07.171
0925-8388/

temperature-sensitive plastic substrates and yet is one of the most important encumbrances restricting the applicability of the solution-processed MOSs.

Recent efforts by the pioneering researchers have led to significant development in lowering the preparation temperature of the solution-processed MOSs by solution combustion process [13], ultraviolet irradiation [14], post-annealing process optimization [15], and so on. Among them, solution combustion process is a new sol-gel exothermic reaction that uses fuel and oxidizer ligands as precursors, and is usually used to prepare the channel layer in the thin-film transistors [13,16–19]. A temperature as low as 200 °C is enough to ignite the combustion reaction. The heat generated during the combustion process of the precursors could help to decompose the organic residuals and accelerate the metal–oxide condensation. Kang et al. optimized the composition ratio of combustible In to Zn precursors and obtained low-resistivity IZO films at 350 °C [20]. More recently, we have attempted to use the solution combustion process to synthesize transparent conductive MOS films at a temperature of 250 °C [21]. But the unavoidable impurity residual made the resulting films exhibit a high resistivity of 40 Ω cm.

Deep ultraviolet (DUV) laser irradiation, which offers rapid and precise energy delivery in area and depth, is recognized as a powerful tool for improving the conductivity of MOSs [16,22–27]. DUV laser irradiation possesses highly desirable features of noncontact processing, high accuracy, fast speed, and low thermal budget. Although considerable attention has been paid in improving the quality of solution-processed MOS films via optimizing the number of impinging shots, pulse repetition frequency, and laser power density, the trade-off between the low annealing temperature and high conductivity is still undesirable. That is because the low-temperature annealed MOS precursors do not absorb the energy of DUV laser. There is still a strong demand for ideal approaches that enable the formation of solution-processed transparent and highly conductive MOS films at low temperature.

It is known that the solution combustion process could accelerate the formation of MOSs at relative low temperature, and high-energy photon irradiation could efficiently degrade the organic molecules. However, the combination usage of DUV irradiation with solution combustion process to fabricate transparent conductive MOS films, which will potentially overcome the abovementioned shortcomings, is rarely exploited up to date. In this study, highly conductive and transparent IZO films were prepared by combining DUV excimer laser radiation with solution combustion sol-gel method at low temperature. The dependency of microstructures, surface morphologies, optical and electrical properties of the IZO films on the DUV excimer laser energy densities was systematically investigated. The IZO films with resistivity as low as 4.2×10^{-3} Ω cm and average transmittance as high as 91% were prepared at 200 °C. We demonstrated that both the removal of residual organic matters and hydroxyl groups and the increase of the percentage of metal–oxygen–metal (M–O–M) bonds contribute to the improvement of optoelectronic performance of the IZO films.

2. Experimental

2.1. Preparation of IZO films

IZO precursor solution was prepared by separately dissolving zinc acetylacetonate hydrate ($Zn(C_5H_7O_2)_2 \bullet xH_2O$, 99.99%) and indium nitrate hydrate ($In(NO_3)_3 \bullet xH_2O$, 99.99%) in anhydrous 2-methoxyethanol ($CH_3OCH_2CH_2OH$, anhydrous 99.8%) solvent, metal precursors were prepared at molar concentration of 0.3 M. All chemicals were purchased from Sigma-Aldrich. The experimental scheme is illustrated in Fig. 1. The procedure can be described as three steps. The precursor solution was agitated at 500 rpm for 12 h at room temperature and then aged over 24 h to prepare the homogeneous solution. The total IZO solution was obtained by mixing the molar ratio of In precursor: Zn precursor at 3 : 1. The precursor solution was spin-coated on a quartz substrate. The spin-coating process was performed at a speed of 2000 rpm for 30 s. The precursor film was dried on a hot plate at 120 °C for 10 min to remove the residual solvent. After five cycles of spin-coating and drying procedures, the resulting IZO films were annealed at 200 °C for 1 h. During the annealing process, a highly intense exothermic reaction occurred. The evolved heat can provide supplemental energy to accelerate the transformation of metal hydroxides or alkoxides into the amorphous IZO frameworks. Then the solution combustion synthesized IZO films were irradiated with DUV KrF excimer laser (λ = 248 nm) at room temperature in the atmospheric environment. The pulse duration of excimer laser was 20 ns, the number of impinging shots was 200 with a frequency of 10 Hz. The laser beam was a rectangular shape (2×4 cm^2) with the energy density varied from 75 to 150 mJ/cm^2. The size of our sample was 2×2 cm^2. The uniformity of the films was checked by dividing the sample into four part. The process reliability of our approach was further verified by repeated fabrication of IZO film for 5 times. The sheet resistance of each part and batch was measured with four-probe system. Their approximately equal sheet resistances confirmed the sample uniformity and method reliability. The IZO films prepared with precursors composed of zinc nitrate and zinc acetate were non-conductive, and thus the IZO films discussed in this following were prepared with precursor composed of zinc acetylacetonate if not specially mentioned.

2.2. Characterization of IZO films

To investigate the thermal behaviour of the IZO films, thermogravimetric analysis (TGA) and differential thermal analysis (DTA, NETZSCH STA 449C) were implemented at a heating rate of 10 °C min^{-1}. The crystal structure of the IZO films was characterized by X-ray diffraction (XRD) using D/max 2500 XRD diffractometer (Rigaku). Scanning electron microscope equipped with EDX (SEM, Quanta 250 FEG) and atomic force microscope (AFM, Bruker Dimension Icon) were used to characterize the morphologies and compositions of the IZO films. Fourier-transform infrared spectra (FT-IR, Thermo Fisher Scientific IS10 spectrometer) were measured to detect the organic impurities. The surface chemical states of the IZO films were analysed using X-ray photoelectron spectroscopy (XPS, VG ESCALAB LKII) with Mg KR-ADES source. The optical transmission spectra of the quartz substrate and IZO films were characterized by the UV−vis spectrophotometer (UH4150, Hitachi). The electrical properties including electron concentration, mobility, and resistivity of the IZO films were measured by a Lakeshore 7704 Hall effect system in the van der Pauw configuration. The thickness of the IZO films were measured with a surface profiler (KLA-Tencor Corp. USA, Alpha-Step D-120).

3. Results and discussion

To investigate the spontaneous exothermic reactions of the fuel and oxidizer ligands, we conducted thermogravimetric analysis (TGA) and differential thermal analysis (DTA) on various zinc precursors. The oxidizer was indium nitrate. TGA and DGA curves for the precursors of zinc nitrate and indium nitrate were shown in Fig. 2a. There was no obvious exothermic peak in the DGA thermogram. The TGA curve shows that there was a mass loss at the temperature range of 50−300 °C. The precursors of zinc acetate and indium nitrate exhibited a similar behaviour (Fig. 2b). The initial mass loss which occurred in the temperature range of 50−200 °C

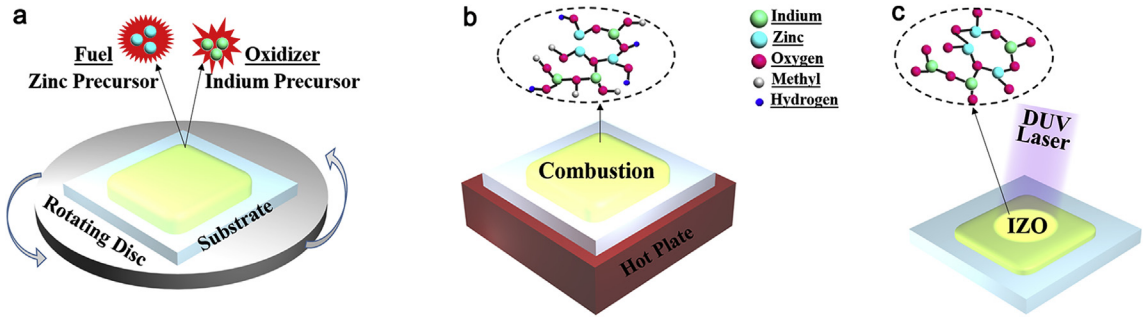

Fig. 1. Schematic of the preparation process of IZO films.

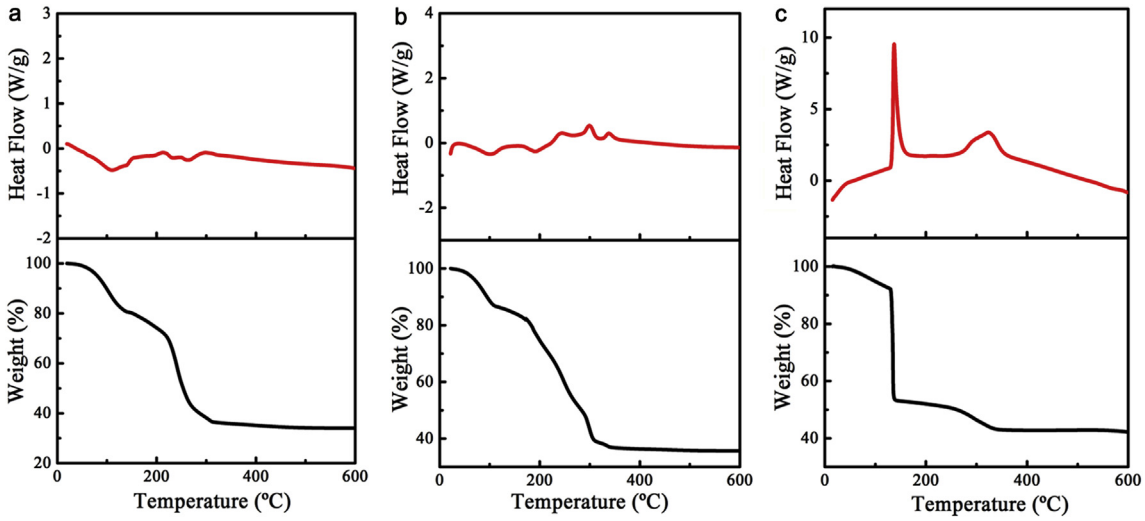

Fig. 2. Thermogravimetric analysis and differential thermal analysis of IZO precursors composed of indium nitrate and various Zn precursors, (a) zinc nitrate, (b) zinc acetate, and (c) zinc acetylacetonate.

originated from the dehydration of the precursors and the volatilization of the solvent. Another weight loss occurred at the temperature range of 200–300 °C was ascribable to the conversion of metal hydroxide to metal oxide via condensation, dehydroxylation, polycondensation, and pyrolysis of the organic components [10]. It was found from the TGA thermogram that a temperature higher than 300 °C was required to form M–O–M lattice for the conventional precursors. In contrast, when the precursors of zinc acetylacetonate and indium nitrate were used, both an intense exothermic peak and a tremendous mass loss were observed at 140–160 °C (Fig. 2c). The weight of precursors was reduced by about 50% before the temperature reached to 200 °C. These phenomena were attributed to the removal of the organic components by the combustion exothermic process of the precursors [6]. It is noteworthy that a broad exothermic peak in the range of 300–350 °C was observed, suggesting a small mass loss related to the dehydroxylation, densification, alloying reaction, and decomposition of the residual organic ligands [13].

The absorption coefficient of the MOS films to the incident laser is an important parameter while converting the photon energy from a laser to heat. Fig. 3a shows the transmission spectrum in the UV light range of the solution combustion synthesized IZO film before DUV excimer laser irradiation. For comparison, the transmission spectrum of the quartz substrate is also shown. According to the equation $\alpha = (1/d)\ln[1/T]$, where d is the thickness and T represents the measured transmittance, respectively. The absorption coefficient (α) of the original IZO film was calculated to be $6.7 \times 10^4\ cm^{-1}$ which is almost four orders higher than that of the quartz glass substrate. Therefore, the photon energy of the excimer laser could be absorbed mostly by the IZO film, which could instantaneously raise the temperature of the IZO film. Theoretically, the temperature of IZO film and its substrate can be calculated by using $\Delta T = \alpha E/C\rho$ in the adiabatic model, where E is the energy density of DUV excimer laser, α, C and ρ is the absorption efficient, specific heat, and density, respectively [28]. The subscripts 1 and 2 represents substrate and IZO film, respectively. First, we calculated the temperature rise (ΔT_1) of a 30 μm thick polymethylmethacrylate (PMMA) substrate under DUV excimer irradiation. For the PMMA substrate with $\alpha_1 = 1.6 \times 10^3\ cm^{-1}$ in the DUV range, $C_1 = 2\ J\ g^{-1}\ K^{-1}$, $\rho_1 = 1.5\ g\ cm^{-3}$, $\Delta T_1 = 66\ K$. Second, we calculated $\Delta T_2 = 1429\ K$, where $\alpha_2 = 6.7 \times 10^4\ cm^{-1}$, $C_2 = 0.837\ J\ g^{-1}\ K^{-1}$, $\rho_2 = 7.0\ g\ cm^{-3}$. Finally, we calculated the temperature rise (ΔT_1) of substrate caused by the heat transferred from IZO film. ΔT_1 can be calculated with $\Delta T_1/\Delta T_2 = C_2\ \rho_2\ h_2/C_1\ \rho_1\ h_1$, where h represents the thickness, $\Delta T_1 = 5.6\ K$. Therefore, the possible temperature rise of the substrate ($\Delta T_1 + \Delta T_1$) was 73 K, indicating that the plastic substrates can survive DUV excimer laser irradiation.

Fig. 3b shows the XRD patterns of the DUV excimer laser-irradiated IZO films. The energy density of the DUV excimer laser varied from 75 to 150 mJ/cm^2. There was no diffraction peak when the laser energy density was less than 100 mJ/cm^2, suggesting that the IZO film was amorphous in this laser energy range. A weak In_2O_3 (222) diffraction peak was observed at the laser energy

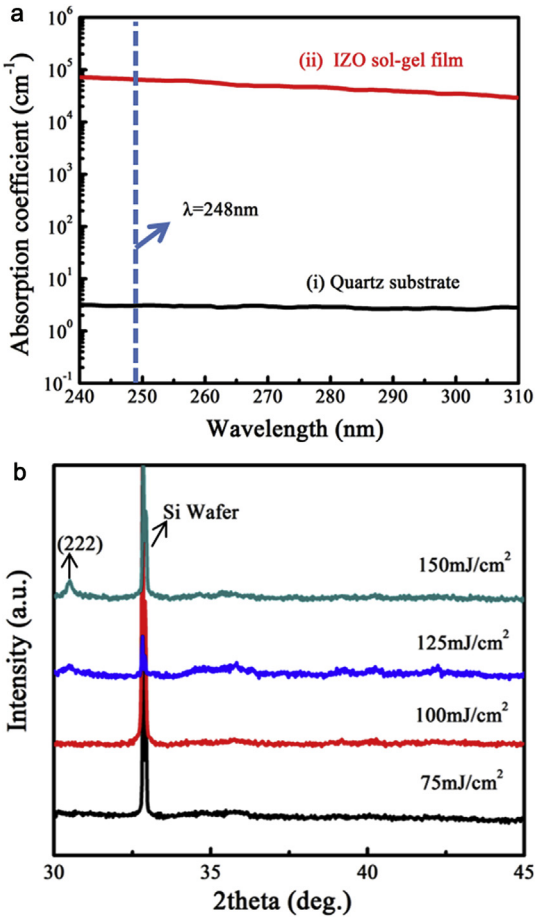

Fig. 3. (a) XRD patterns of the solution combustion synthesized IZO films irradiated with different DUV excimer laser energy densities. (b) Absorption spectra of the solution combustion synthesized IZO film and the quartz substrate in the UV light range.

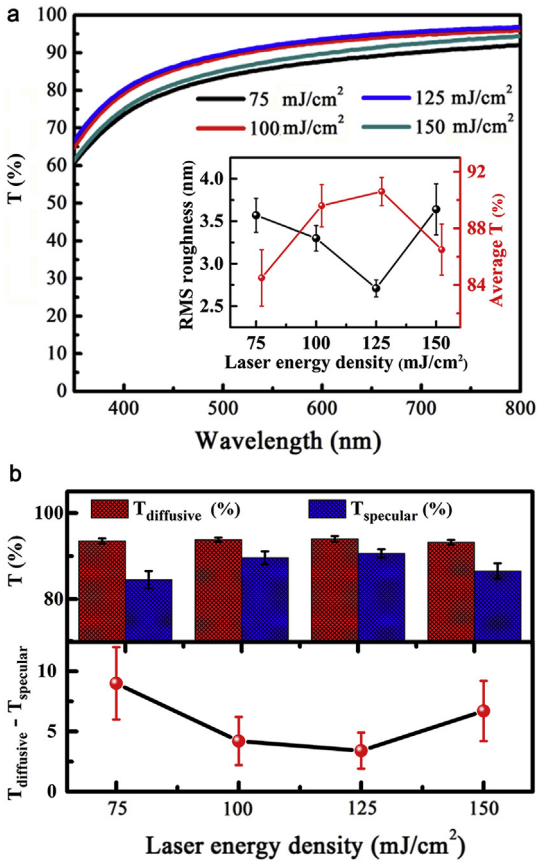

Fig. 5. (a) Optical transmission spectra in the visible light region of the IZO films irradiated with different laser energy densities, (b) corresponding average diffusive ($T_{diffusive}$) and specular transmittance ($T_{specular}$), and the difference between them ($T_{diffusive} - T_{specular}$). The inset in (a) is the RMS surface roughness and average transmittance of the DVU excimer laser-irradiated IZO films at different energy densities.

density of 125 mJ/cm^2, indicating that a small amount of In_2O_3 nanocrystals were formed in the amorphous IZO films. As the laser energy density increased to 150 mJ/cm^2, the crystallization of In_2O_3 was enhanced and its diffraction peak became stronger. Nakata et al. have numerically estimated that the temperature of the laser-irradiated MOS film increased exponentially with the increase of the laser energy density [28]. The high absorption coefficient of the IZO film enabled them to absorb most of the incident DUV photon and convert the photon energy into the phonon energy. Thus, increasing the DUV excimer laser energy density raised the IZO films temperature and led to the precipitation of a small number of In_2O_3 nanocrystals.

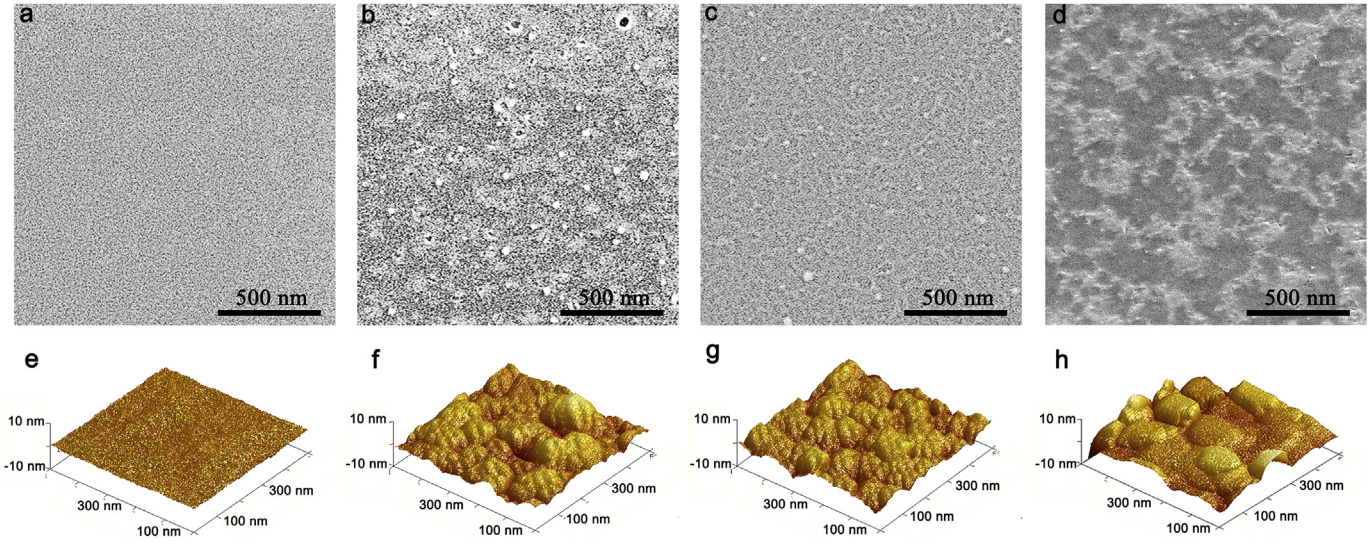

Fig. 4. SEM (a–d) and the corresponding AFM (e–h) micrographs of the IZO films irradiated with the DUV excimer laser density of 0, 100, 125, and 150 mJ/cm^2, respectively.

The surface morphology of the IZO films changing with the DUV excimer laser energy densities was characterized by scanning electron microscope (SEM) and atomic force microscope (AFM). Fig. 4a–d and 4e–h show the SEM and AFM images of the IZO films obtained at laser energy densities of 0, 100, 125 and 150 mJ/cm^2, respectively. As shown in Fig. 4a and e, the surface of the solution combustion synthesized IZO film was smooth and void-free, with a low root-mean-square (RMS) surface roughness of 0.35 nm. Fig. 4b and f show that the IZO film surface became rough and the RMS surface roughness reached to 3.3 nm after 100 mJ/cm^2 laser irradiation. We further measured the thickness of the film by using a step profiler. It is found that the thickness of the IZO films decreased from 80 to 62 nm after the laser irradiation. The increase of the RMS surface roughness after laser irradiation can be attributed to the removal of the organic matters and the tensile stress induced by the rapid cooling after the laser annealing. When the laser energy density increases to 125 mJ/cm^2, the RMS surface roughness decreased to 2.7 nm, which can be attributed to the densification of the IZO film (Fig. 4c and g). However, as the laser energy density increased to 150 mJ/cm^2, some pinholes appeared on the surface of IZO film and the RMS surface roughness was back to 3.6 nm (Fig. 4d and h) due to the surface re-evaporation and the precipitation of In_2O_3 nanocrystals. Additionally, the composition of IZO films was analysed by using EDX. The actual atomic concentrations of indium incorporated in the films were different from the starting values and changed with the DUV excimer laser densities. At 100, 125 and 150 mJ/cm^2, the actual atomic concentrations of indium ([In]/[Zn + In]) was 0.65, 0.44 and 0.38, respectively. The concentration of In varied with DUV excimer laser densities is probable due to evaporation of In Refs. [29,30].

The surface morphologies make a significant influence on the optical transmittance of the IZO films. Fig. 5a shows the specular transmission spectra of the IZO films irradiated by 0–150 mJ/cm^2 laser energy densities. The red line in the inset shows the average transmittance versus the laser energy density, in which all the IZO films have an average transmittance higher than 84% in the visible region. At the energy density of 125 mJ/cm^2, the IZO film exhibited the highest visible transmittance of 91%. The black line in the inset of Fig. 5a shows the dependence of the RMS surface roughness on the laser energy density. We found that the variation trend of the average specular transmittance was opposite to that of the RMS surface roughness. These phenomena are reasonable because the IZO films with rough surface scattered more visible light than the flat ones. The difference between the diffusive transmittance and the specular transmittance ($T_{diffusive} - T_{specular}$) confirmed the above explanations. As shown in Fig. 5b, the diffusive transmittances were comparable for all the IZO films. The IZO film irradiated by 125 mJ/cm^2 laser energy showed the lowest ($T_{diffusive} - T_{specular}$). The IZO film irradiated by 150 mJ/cm^2 DUV excimer laser exhibited lower specular transmittance than that of 125 mJ/cm^2. These results are consistent with the previous report [29], and was attributed to the enhanced light scattering of the IZO film irradiated with high-energy DUV excimer laser.

To investigate the effects of DUV excimer laser irradiation on the bonding states in IZO films, Fourier-transform infrared (FT-IR) spectra and X-ray photoelectron spectra (XPS) analyses were conducted. Fig. 6a shows the FT-IR spectra of the solution combustion synthesized IZO films without and with 125 mJ/cm^2 laser irradiation. The broad peaks at 3430, 1588, and 1296 cm^{-1} were related to the O–H and C–O stretching vibrations, COO^- asymmetric vibration, respectively [11]. The vibration modes at 2943 and 2836 cm^{-1} were assigned to the symmetric and asymmetric C–H stretching vibration [5]. In contrast, the DUV excimer laser-irradiated IZO film did not show any C–H, C–O, COO^- or O–H vibrations. Based on these results, we confirmed that DUV excimer laser irradiation effectively removed the carbon and hydroxyl bonds in the solution

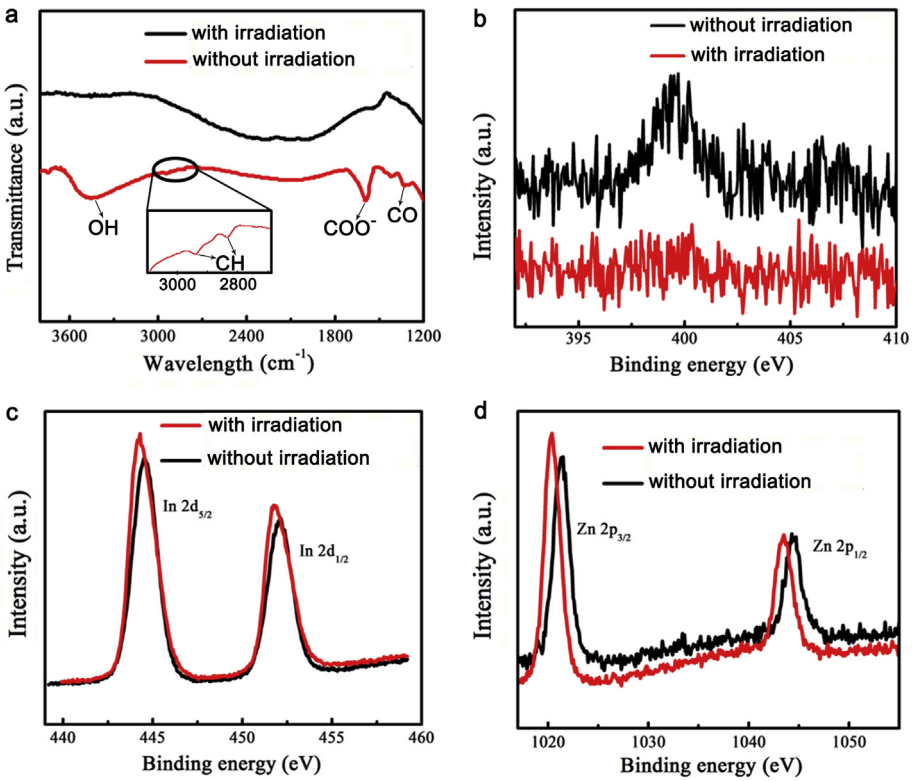

Fig. 6. (a) FT-IR spectra, and (b–d) N 1s, In 2d, and Zn 2p XPS of the solution combustion synthesized IZO films without and with DUV excimer laser irradiation, respectively.

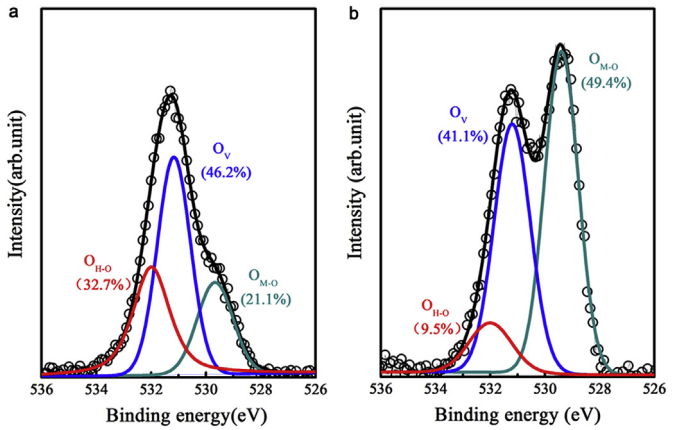

Fig. 7. O 1s XPS of the solution combustion synthesized IZO films without (a) and with (b) DUV excimer laser irradiation.

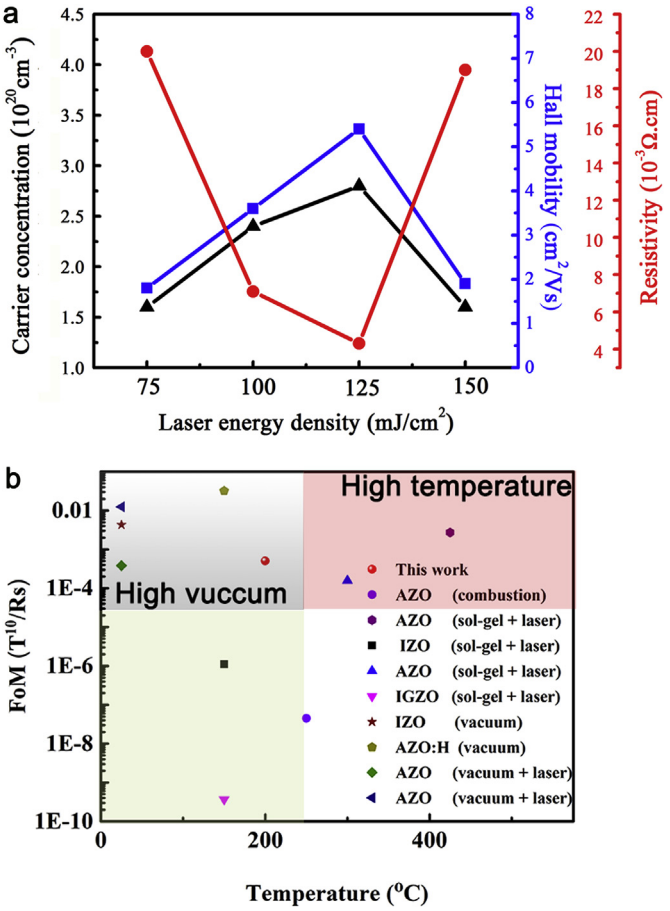

Fig. 8. (a) Variation of the carrier concentration, Hall mobility, and resistivity with the DUV excimer laser energy densities of the IZO films. (b) Fabrication temperature dependence of the FoM of the landmark MOS transparent conductors reported in the literature [10,11,21,23,25,29,43–45].

combustion synthesized IZO films. Fig. 6b shows that N 1s peak in the IZO film disappeared after excimer laser irradiation, suggesting that DUV excimer laser can effectively decompose the nitrate compounds in the IZO films. Fig. 6c and d show that the In $3d_{2/5}$ and Zn $2p_{3/2}$ peaks, which are known to be located at 444.6 and 1021.5 eV and represented the In—O and Zn—O bonds for the IZO film [30,31], shifted to lower energy of 444.1 and 1020.4 eV after the DUV excimer laser irradiation, respectively. Choi et al. observed a similar peak shift towards low-bonding energy with increasing thermal annealing time [32]. Those phenomena are related to the improved crystallographic structures of IZO and the enhanced bonding between the metal and oxygen atoms.

Fig. 7a and b show the O 1s XPS of the solution combustion synthesized IZO films without and with DUV excimer laser irradiation, respectively. The Gaussian function was used to complete the deconvolution of the O 1s XPS peaks. The three components, located at 529.5 ± 0.2, 531.2 ± 0.2, and 532 ± 0.2 eV, were assigned to the M–O–M bonds, oxygen vacancies, and hydroxyl group, respectively [13,33–36]. The three types of O composition in the IZO films were calculated based on the ratio of the integrated areas of each O 1s peak to that of the total O 1s peak. We found that the solution combustion synthesized IZO film contained many hydroxyl groups before the laser irradiation, which agrees well with our observations in the FT-IR spectra. After the laser irradiation, the percentage in M–O–M bonds increased from 21.1% to 49.4%, and the percentage in M–OH bonds decreased from 32.7% to 9.5%. These results demonstrate that DUV excimer laser irradiation converts the M–OH bonds into M–O–M bonds efficiently. Because the hydroxy groups in the IZO films can work as the scattering centers [37], decreasing the number of hydroxy groups can improve the carrier mobility of the IZO films, as we will discuss below.

Variations of the carrier concentration, Hall mobility, and resistivity of the IZO films with laser energy density are shown in Fig. 8a. The solution combustion synthesized IZO film was insulative and its data were not listed here. The carrier concentration and carrier mobility increased with increasing DUV excimer laser energy densities (from 75 to 125 mJ/cm^2). Further, the carrier concentration and carrier mobility of the IZO films decreased with increasing DUV excimer laser energy density. A minimum resistivity of $4.2 \times 10^{-3}\ \Omega$ cm was obtained at the laser energy density of 125 mJ/cm^2. These results are consistent with the composition and surface morphology changes with the laser energy densities. As discussed in our previous XPS and XRD analyses, when the DUV excimer laser irradiation is moderate, DUV photons will eliminate the organic residuals in the IZO films due to the photodegradation and photothermal effects. As results, the IZO films will become dense and the number of M–O–M bonds will increase at the same time. The formation of M–O–M bonds is favorable for the s-orbital overlap between adjacent In and Zn atoms, which can provide conducting pathways for electron transportation and improve the electrical conductivity of the IZO films. However, further increasing the DUV excimer laser energy density to 150 mJ/cm^2 led to a deterioration of the conductivity of the IZO film. That is because the DUV excimer laser with large energy density introduce pinholes and In_2O_3 precipitations, which resulted in an increase of the carrier scattering and a decrease of the electron mobility in the IZO films. In addition, the electrical resistivity of the IZO film was measured again after storing in ambient for a month. The resistivity of IZO film increased only by 0.5 times due to the chemisorbed-oxygen and/or water molecules permeation from atmosphere into IZO film through the topmost surface [38]. Compare with the high-temperature annealed polycrystalline AZO film whose resistivity increased by about one time [39], the relatively stability of IZO film was attributed to the nearly nonexistent grain boundaries in amorphous film which may reduce the rate of oxygen and/or water molecule diffusion to the film.

Generally, the transmittance and conductivity of the transparent conducting films may conflict with each other. Thus, it is desirable to achieve a balance between these two competing factors. The Figure of Merit (FoM) can be expressed as follows: $FoM = T^{10}/Rs$, where T is the visible transmittance and Rs is the sheet resistance of

transparent conductors. Higher the FoM means a better optoelectronic performance [40–42]. Considering that the preparation temperature is a key factor that determines the FoM of the solution-processed transparent conductive films, we provide the plot of FoM-temperature in Fig. 8b. For comparison purposes, the calculated FoMs of some landmark transparent conductors are also provided. The IZO film prepared by combining solution combustion process and DUV excimer laser irradiation has a FoM as high as $5 \times 10^{-4}\,\Omega^{-1}$ at a low fabrication temperature of 200 °C. That performance is clearly superior to the AZO film prepared by combustion process at 250 °C without laser irradiation [21], comparable to the AZO film prepared by conventional high temperature sol-gel method with laser irradiation [23], and superior to the IZO [25], AZO [29], and IGZO [43] films prepared by conventional low-temperature sol-gel method with laser irradiation. Although the FoM of our IZO film is lower than some of landmark transparent conductors composed of IZO [10] and hydrogen-doped AZO films [11], the IZO films exhibit comparable optoelectronic performance with the AZO films prepared by high-vacuum magnetron sputtering and DUV laser irradiation thereafter [44,45]. To demonstrate the possibility of preparation of IZO on flexible substrate, we prepared an IZO film on a polyimide substrate by the same procedure as on glass. The resistance of IZO film remained unchanged with a bending radius of 3 cm.

4. Conclusion

In summary, we have developed a method to fabricate highly conductive and transparent amorphous IZO films at low temperature by using solution combustion process and DUV excimer laser irradiation. It was found that the DUV excimer laser irradiation led to removal of organic residuals and hydroxyl groups, as well as increase in the ratio of M–O–M chemical bond in the solution combustion synthesized IZO films. With a laser energy density of 125 mJ/cm^2, an IZO film with carrier mobility of 5.5 cm^2 V^{-1} s^{-1}, resistivity of $4.2 \times 10^{-3}\,\Omega$ cm, visible light transmittance of 91%, and high stability in ambient was obtained at a temperature as low as 200 °C. These results demonstrated that the method developed in this work has great potential to be used in the field of flexible optoelectronics.

Acknowledgments

The work is supported by the National Natural Science Foundation of China (NSFC) (No. 51872043, 51732003, 61574031), "111 Project", china (No. B13013), Key Research Program of Frontier Science, CAS, China (No. QYZDB-SSW-SLH014), Open Research Fund of Key laboratory of UV-Emitting Materials and Technology (No.130028856), the China Postdoctoral Science Foundation (No. 2018M640273), and the Fundamental Research Funds for the Central Universities (No. 2412019QD014), the Fund from Jilin Province, China (No. JJKH20190267KJ).

References

[1] M. Lorenz, M.S.R. Rao, T. Venkatesan, E. Fortunato, P. Barquinha, R. Branquinho, D. Salgueiro, R. Martins, E. Carlos, A. Liu, F.K. Shan, M. Grundmann, H. Boschker, J. Mukherjee, M. Priyadarshini, N. DasGupta, D.J. Rogers, F.H. Teherani, E.V. Sandana, P. Bove, K. Rietwyk, A. Zaban, A. Veziridi, A. Weidenkaff, M. Muralidhar, M. Murakami, S. Abel, J. Fompeyrine, J.Z. Perez, R. Ramesh, N.A. Spaldin, S. Ostanin, V. Borisov, I. Mertig, V. Lazenka, G. Srinivasan, W. Prellier, M. Uchida, M. Kawasaki, R. Pentcheva, P. Gegenwart, F.M. Granozio, J. Fontcuberta, N. Pryds, The 2016 oxide electronic materials and oxide interfaces roadmap, J. Phys. D Appl. Phys. 49 (2016) 433001.
[2] A. Mosbahab, M.S. Aida, Influence of deposition temperature on structural, optical and electrical properties of sputtered Al doped ZnO thin films, J. Alloy. Comp. 515 (2012) 149–153.
[3] Z.Z. You, G.J. Hua, Electrical, optical and microstructural properties of transparent conducting GZO thin films deposited by magnetron sputtering, J. Alloy. Comp. 530 (2012) 11–17.
[4] R. Martins, P. Almeida, P. Barquinha, L. Pereira, A. Pimentel, I. Ferreira, E. Fortunato, Electron transport and optical characteristics in amorphous indium zinc oxide films, J. Non-Cryst. Solids 352 (2006) 1471–1474.
[5] E. Fortunato, R. Martins, Where science fiction meets reality? With oxide semiconductors!, Phys. Status Solidi Rapid Res. Lett. 5 (2011) 336–339.
[6] X.Z. Yan, X. Man, J.G. Ma, H.Y. Xu, Y.C. Liu, Modulation of electron transportation in amorphous and polycrystalline indium–zinc-oxide films grown by pulse laser deposition, J. Non-Cryst. Solids (423–424) (2015) 18–24.
[7] T. Minami, Transparent conducting oxide semiconductors for transparent electrodes, Semicond. Sci. Technol. 20 (2005) S35–S44.
[8] L. Raniero, I. Ferreira, A. Pimentel, A. Gonçalves, P. Canhola, E. Fortunato, R. Martins, Role of hydrogen plasma on electrical and optical properties of ZGO, ITO and IZO transparent and conductive coatings, Thin Solid Films 511–512 (2006) 295–298.
[9] G. Gonçalves, E. Elangovan, P. Barquinha, L. Pereira, R. Martins, E. Fortunato, Influence of post-annealing temperature on the properties exhibited by ITO, IZO and GZO thin films, Thin Solid Films 515 (2007) 8562–8566.
[10] E. Fortunato, A. Pimentel, A. Goncçalves, A. Marques, R. Martins, High mobility amorphous/nanocrystalline indium zinc oxide deposited at room temperature, Thin Solid Films 502 (2006) 104–107.
[11] A. Lyubchyk, A. Vicente, B. Soule, P.U. Alves, T. Mateus, M.J. Mendes, H. Águas, E. Fortunato, R. Martins, Mapping the electrical properties of ZnO-based transparent conductive oxides grown at room temperature and improved by controlled postdeposition annealing, Adv. Electron. Mater. 2 (2016) 1500287.
[12] J.-H. Lee, K.-H. Ko, B.-O. Park, Electrical and optical properties of ZnO transparent conducting films by the sol–gel method, J. Cryst. Growth 247 (2003) 119–125.
[13] M.-G. Kim, M.G. Kanatzidis, A. Facchetti, T.J. Marks, Low-temperature fabrication of high-performance metal oxide thin-film electronics via combustion processing, Nat. Mater. 10 (2011) 382–388.
[14] J.H. Park, S.S. Chae, Y.B. Yoo, J.H. Lee, T.I. Lee, H.K. Baik, Fabrication of solution-processed amorphous indium zinc oxide thin-film transistors at low temperatures using deep-UV irradiation under wet conditions, Chem. Phys. Lett. 597 (2014) 121–125.
[15] K. Jiang, J.T. Anderson, K. Hoshino, D. Li, J.F. Wager, D.A. Keszler, Low-energy path to dense HfO_2 thin films with aqueous precursor, Chem. Mater. 23 (2011) 945–952.
[16] C.-N. Chen, J.-J. Huang, Effects of excimer laser annealing on low-temperature solution based indium-zinc-oxide thin film transistor fabrication, J. Appl. Res. Technol. 13 (2015) 170–176.
[17] Y.H. Kang, S. Jeong, J.M. Ko, J.-Y. Lee, Y. Choi, C. Lee, S.Y. Cho, Two-component solution processing of oxide semiconductors for thin-film transistors via self-combustion reaction, J. Mater. Chem. C 2 (2014) 4247–4256.
[18] Y.S. Rim, H.S. Lim, H.J. Kim, Low-temperature metal-oxide thin-film transistors formed by directly photopatternable and combustible solution synthesis, ACS Appl. Mater. Interfaces 5 (2013) 3565–3571.
[19] J.-W. Choi, S.-Y. Han, M.-C. Nguyen, A.H.-T. Nguyen, J.Y. Kim, S. Choi, J. Cheon, H. Ji, R. Choi, Low-temperature solution-based In_2O_3 channel formation for thin-film transistors using a visible laser-assisted combustion process, IEEE Electron. Device Lett. 38 (2017) 1259–1262.
[20] Y.H. Kang, K.-S. Jang, C. Lee, S.Y. Cho, Facile preparation of highly conductive metal oxides by self-combustion for solution-processed thermoelectric generators, ACS Appl. Mater. Interfaces 8 (2016) 5216–5223.
[21] Y. Wang, M. Xu, J. Li, J. Ma, X. Wang, Z. Wei, X. Chu, X. Fang, F. Jin, Sol-combustion synthesis of Al-doped ZnO transparent conductive film at low temperature, Surf. Coat. Technol. 330 (2017) 255–259.
[22] J. Kim, J.-H. Ji, S.-W. Min, G.-H. Jo, M.-W. Jung, M.-J. Park, S.-K. Lee, J.-H. Koh, Enhanced conductance properties of UV laser/RTA annealed Al-doped ZnO thin films, Ceram. Int. 43 (2017) 3900–3904.
[23] Q. Nian, M. Callahan, D. Look, H. Efstathiadis, J. Bailey, G.J. Cheng, Highly transparent conductive electrode with ultra-low HAZE by grain boundary modification of aqueous solution fabricated alumina-doped zinc oxide nanocrystals, Apl. Mater. 3 (2015) 062803.
[24] K. Kim, S. Kim, S.Y. Lee, Effect of excimer laser annealing on the properties of ZnO thin film prepared by sol-gel method, Curr. Appl. Phys. 12 (2012) 585–588.
[25] C.-Y. Tsay, T.-T. Huang, Characterization of low-temperature solution-processed indium–zinc oxide semiconductor thin films by KrF excimer laser annealing, Ceram. Int. l40 (2014) 8287–8292.
[26] M. Nakata, K. Takechi, T. Eguchi, E. Tokumitsu, H. Yamaguchi, S. Kaneko, Flexible high-performance amorphous $InGaZnO_4$ thin-film transistors utilizing excimer laser annealing, Jpn. J. Appl. Phys. 48 (2009) 081607.
[27] C.-Y. Tsay, K.-S. Fan, C.-M. Lei, Synthesis and characterization of sol–gel derived gallium-doped zinc oxide thin films, J. Alloy. Comp. 512 (2012) 216–222.
[28] R. Branquinho, D. Salgueiro, L. Santos, P. Barquinha, L. Pereira, R. Martins, E. Fortunato, Aqueous combustion synthesis of aluminum oxide thin films and application as gate dielectric in GZTO solution-based TFTs, ACS Appl. Mater. Interfaces 6 (2014) 19592–19599.
[29] W.M. Tsang, F.L. Wong, M.K. Fung, J.C. Chang, C.S. Lee, S.T. Lee, Transparent conducting aluminum-doped zinc oxide thin film prepared by sol–gel process followed by laser irradiation treatment, Thin Solid Films 517 (2008) 891–895.

[30] Y.S. Jung, J.Y. Seo, D.W. Lee, D.Y. Jeon, Influence of DC magnetron sputtering parameters on the properties of amorphous indium zinc oxide thin film, Thin Solid Films 445 (2003) 63–71.
[31] D.-G. Kim, S. Lee, D.-H. Kim, G.-H. Lee, M. Isshiki, Temperature dependence of the microstructure and resistivity of indium zinc oxide films deposited by direct current magnetron reactive sputtering, Thin Solid Films 516 (2008) 2045–2049.
[32] J.H. Choi, J.H. Shim, S.M. Hwang, J. Joo, K. Park, H. Kim, H.-J. Lee, J.H. Lim, M.R. Moon, D. Jung, Effect of sintering time at low temperature on the properties of IGZO TFTs fabricated by using the sol-gel process, J. Korean Phys. Soc. 57 (2010) 1836–1841.
[33] Y.J. Tak, S.P. Park, T.S. Jung, H. Lee, W.-G. Kim, J.W. Park, H.J. Kim, Reduction of activation temperature at 150 °C for IGZO films with improved electrical performance via UV-thermal treatment, J. Inf. Disp. 17 (2016) 73–78.
[34] M. Fujii, Y. Ishikawa, R. Ishihara, J.V.D. Cingel, M.R.T. Mofrad, M. Horita, Y. Uraoka, Low temperature high-mobility InZnO thin-film transistors fabricated by excimer laser annealing, Appl. Phys. Lett. 102 (2013) 122107.
[35] S.S. Sanctis, J. Krausmann, C. Guhl, J.J. Schneider, Stacked indium oxide/zinc oxide heterostructures as semiconductors in thin film transistor devices: a case study using atomic layer deposition, J. Mater. Chem. C 6 (2018) 464–472.
[36] S. Jeong, Y.-G. Ha, J. Moon, A. Facchetti, T.J. Marks, Role of gallium doping in dramatically lowering amorphous–oxide processing temperatures for solution-derived indium zinc oxide thin–film transistors, Adv. Mater. 22 (2010) 1346–1350.
[37] P. Li, H. Li, J. Ma, Y. Zhou, W. Zhang, L. Cong, H. Xu, Y. Liu, Structural optimization of oxide/mmetal/oxide transparent conductors for high–performance low–emissivity heaters, Adv. Mater. Interfac. 5 (2018) 1801287.
[38] T.L. Chen, D.S. Ghosh, D. Krautz, S. Cheylan, V. Pruneri, Highly stable Al-doped ZnO transparent conductors using an oxidized ultrathin metal capping layer at its percolation thickness, Appl. Phys. Lett. 99 (2011) 093302.
[39] S. Tabassum, E. Yamasue, H. Okumura, K.N. Ishihara, Electrical stability of Al-doped ZnO transparent electrode prepared by sol-gel method, Appl. Surf. Sci. 377 (2016) 355–360.
[40] G. Haacke, New figure of merit for transparent conductors, J. Appl. Phys. 47 (1976) 4086.
[41] P. Li, W. Zhang, J. Ma, X. Wang, H. Xu, L. Cong, Y. Liu, Solution–grown serpentine silver nanofiber meshes for stretchable transparent conductors, Adv. Electron. Mater. 4 (2018) 1800346.
[42] P. Li, J.G. Ma, H.Y. Xu, D. Lin, X.D. Xue, X.Z. Yan, P. Xia, Y.C. Liu, Flexible transparent heaters based on silver nanotrough meshes, J. Alloy. Comp. 664 (2016) 764–769.
[43] C.-Y. Tsay, T.-T. Huang, Improvement of physical properties of IGZO thin films prepared by excimer laser annealing of sol–gel derived precursor films, Mater. Chem. Phys. 140 (2013) 365–372.
[44] C.-F. Ding, W.-T. Hsiao, H.-T. Young, Effect on the electro-optical properties of transparent conducting aluminum doped zinc oxide thin films using low temperature ultraviolet laser annealing, J. Mater. Sci. Mater. Electron. 28 (2017) 15647–15656.
[45] S.O. Elhamali, W.M. Cranton, N. Kalfagiannis, X. Hou, R. Ranson, D.C. Koutsogeorgis, Enhanced electrical and optical properties of room temperature deposited Aluminium doped Zinc Oxide (AZO) thin films by excimer laser annealing, Opt. Lasers Eng. 80 (2016) 45–51.